Ice basin experiments on mixed-mode failure on ice cones

Petry, Alice; Hammer, Tim C.; Polojärvi, Arttu; Hendrikse, Hayo; Puolakka, Otto

Publication date
2023

Document Version
Final published version

Published in
Proceedings of the 27th International Conference on Port and Ocean Engineering under Arctic Conditions

POAC'23
Glasgow, United Kingdom

Proceedings of the 27th International Conference on
Port and Ocean Engineering under Arctic Conditions
12-16 June 2023, Glasgow, United Kingdom

Ice basin experiments on mixed-mode failure on ice cones

Alice Petry[1], Tim C. Hammer[2], Arttu Polojärvi[1], Hayo Hendrikse[2], Otto Puolakka[1]

[1] Aalto University, School of Engineering, Department of Mechanical Engineering, Espoo, Finland

[2] Delft University of Technology, Department of Hydraulic Engineering, Delft, The Netherlands

ABSTRACT

Increased activity in planning offshore wind farms in the northern Baltic Sea has renewed interest in studying the effect of ice cones on ice failure mechanisms. In preparation for future experiments with steep ice cones, preliminary ice basin experiments were performed at the Aalto Ice and Wave Tank to investigate how model ice fails against a 3D-printed cylindrical and a conical structure representative of wind turbine foundations. The main motivation behind the two structures is to test ice loads on a monopile foundation and a monopile foundation fitted with an upward-bending ice cone. Each structure was tested at eight different velocities in three ice sheets with varying mechanical properties, including a newly developed, crushing-optimized model ice. The force exerted by the ice on these rigid structures was measured using a six-axis load cell. The results show that ice undergoes mixed-mode failure on the cone in the form of bending, crushing, and spalling, when tested in crushing-optimized ice. Based on the observations and results, it is recommended that model-scale experiments, focused on mixed-mode ice failure, use model ice with a representative compressive to flexural strength ratio, scaled flexural and compressive strength, and the ability to fail in brittle crushing. If these criteria cannot be met, it may be possible to combine test results from different ice sheets, each focused on one ice failure mechanism. Additionally, this study successfully used 3D-printed structures, which present a new and more accessible method of preparing scale models.

KEY WORDS: Model-scale experiments; Ice-structure interaction; Ice cone; Offshore wind.

INTRODUCTION

Offshore wind power is a key renewable energy resource in Europe's green transition. Currently, the Baltic Sea has an installed capacity of 2.8 GW, that is set to be increased to 19.6 GW by 2030 (WindEurope, 2022). However, the presence of sea ice makes the expansion of wind energy production to the northern Baltic challenging. Sea ice can lead to high static and dynamic loads on offshore structures, as has been observed on Molikpaq platform (Cornett & Timco, 1998), a monopod structure in Bohai Bay (Yue et al., 2009), and the Norströmsgrund lighthouse (Nord et al., 2018). Considering that offshore wind turbines are slender and compliant structures, they are likely to experience severe ice-induced vibrations (Hammer et al., 2023).

To mitigate the risk of ice-induced vibrations, offshore wind turbine foundations can be fitted with an ice cone, a conical structure that forces ice to fail in bending. Despite their effectiveness in reducing ice loads, ice cones lead to higher material, transport, and installation costs due to their added weight and larger volume. This also leads to increased ice

loads when interacting with ridges and increased wave loads during ice-free seasons. These factors make ice cones less appealing for offshore wind projects that typically utilize monopile foundations. Some of these issues could be mitigated by using smaller and steeper ice cones. Steep cones may, however, lead to mixed-mode ice failure characterized by a combination of crushing and flexural failure.

Few ice basin tests have been performed with steep ice cones. Jiang et al. (2021) tested a 75-degree upward-bending cone moving through a ridge, Ziemer et al. (2015) tested an 80-degree upward-bending cone and Saeki at al. (1996) tested a 75-degree upward bending cone. From these, Ziemer et al. (2015) are the only ones to describe the ice failure process. They reported that the dominant failure mode was flexural failure accompanied by short periods of crushing at low velocities. More recent experimental studies focused on analyzing ice-induced vibrations of wind turbines with monopile foundations instead of ice cones (Hendrikse et al., 2022a; Tian et al., 2019). Hendrikse et al. (2022b) tested a cylindrical pile using "cold-top" model ice, a crushing-optimized model ice developed at the Aalto Ice and Wave Tank. Hamburg Ship Model Basin also developed a model ice with better ice crushing properties (Ziemer et al., 2022). These new types of model ice have led to improved model-scale experiments focused on ice crushing against vertical structures, but they have not yet been tested against ice cones.

In preparation for future ice basin tests with steep cones, preliminary experiments were performed at Aalto Ice and Wave Tank. The aim of these experiments was to investigate the effects of varying mechanical properties of model ice on the failure process when tested against two types of structures: a cylindrical structure representative of a monopile foundation, and a monopile foundation equipped with an ice cone. In addition, this study tested the use of 3D-printed structure models in ice basin tests.

METHODOLOGY

Ice basin experiments were performed in December 2022 and January 2023 at the Aalto Ice and Wave Tank. The basin measures 40 m × 40 m in area and 2.8 m in depth. It is spanned by a bridge that holds a carriage, which can move at various speeds across the basin (Figure 1).

Figure 2 shows the test setups with the cylinder and cone structure models. The cylinder has an outer diameter of 300 mm. The cone is an upward-bending cone with a 60-degree slope angle. It has a waterline diameter of 400 mm with cylindrical extensions above and below

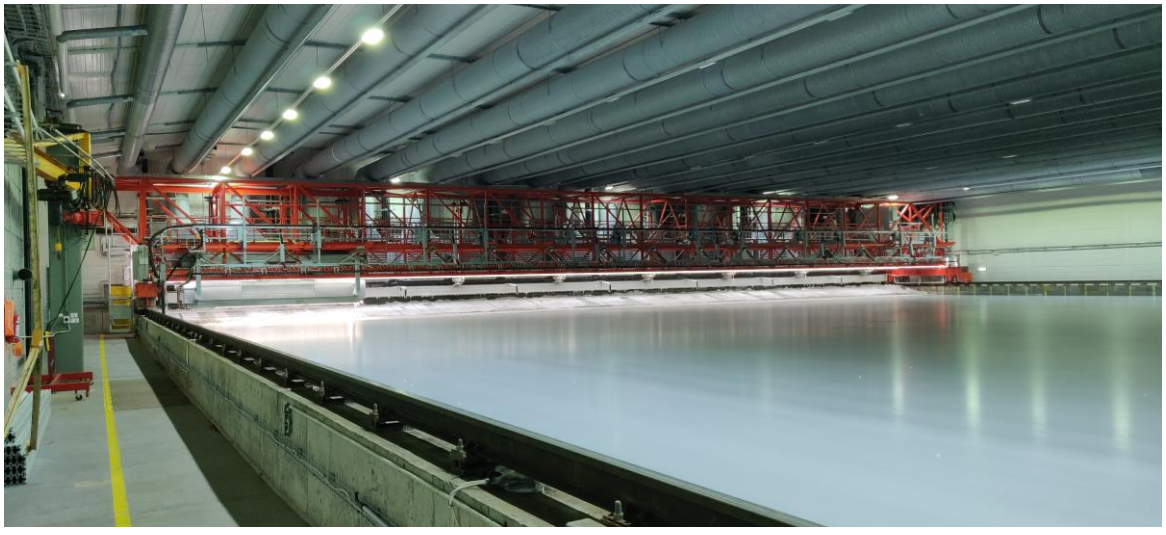

Figure 1. Aalto Ice and Wave Tank.

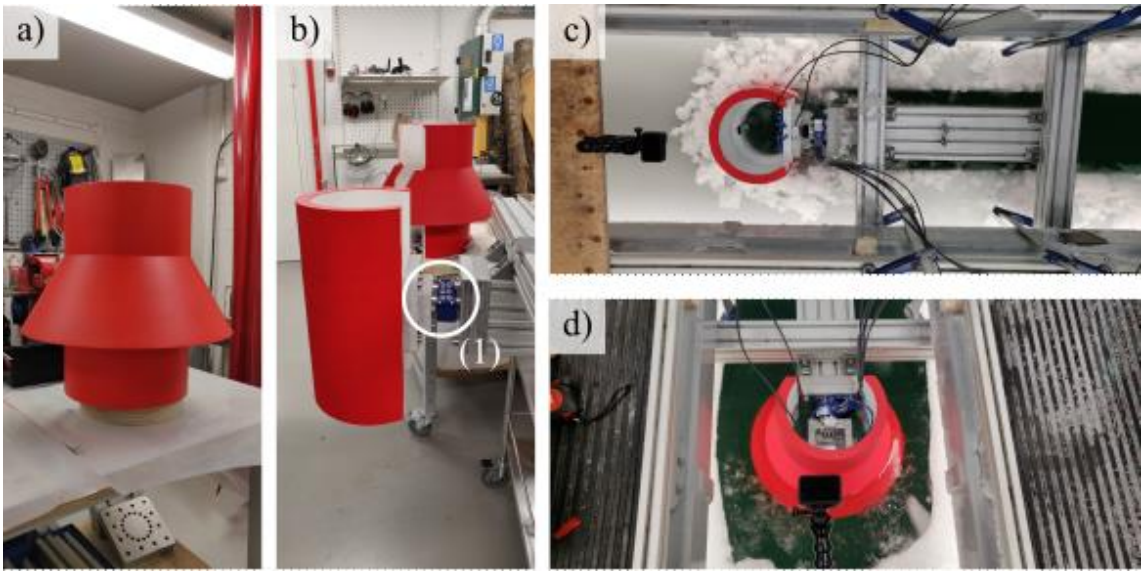

Figure 2. Test setup and instrumentation: a) cone model; b) cylinder model attached to (1) loadcell; c) test setup with cylinder model and d) with cone model in the ice basin.

with a diameter of 300 mm. The ratio of waterline diameter to ice thickness is 10. Both structures have a height of 47 cm. The 3D-printed structure models were attached to an aluminum frame. A six-axis load cell (HBM MCS10-10kN) was placed between the structure and the frame (Figure 2 b). The test setup was clamped to the floor opening of the carriage in the ice basin and the carriage moved during the experiments (Figure 2 c and d). When the cylinder and cone models were submerged up to the designated water line, their natural frequencies were 165 Hz and 180 Hz, respectively. The frequencies are high enough to consider the setup rigid. These natural frequencies were measured using accelerators placed close to the load cell and inside the structure models.

Three different ice sheets were tested (Table 1): “standard”, “strong”, and “cold” model ice. The ethanol-doped fine-grained model ice was produced according to the techniques described in (Li & Riska, 1996). To grow the ice, the ethanol-water mixture was sprayed layer-by-layer as a mist at an ambient temperature of –10 to –16 ℃ until the target ice thickness was reached. Next, it was frozen at a suitable ambient temperature to reach the desired ice strength. During the experiments, the ambient temperature was increased to between +0 to +2 ℃ for “standard” and “strong” model ice, while it was kept at –11 ℃ for “cold” model ice. The ice properties were tested in two locations along the test track: once before testing with the cone and again before testing with the cylinder. Both structures were tested at constant velocities 5, 6, 7, 8, 9, 10, 20, and 50 mm/s over 3 m each. Note that the experimental setup was not scaled in according with scaling conventions. Nonetheless, geometric scaling can be applied using a factor λ=20-30 to help interpret the results.

Table 1. Ice properties measured on testing days before cone and cylinder tests.

Ice type	Thickness [mm]	Flexural strength [kPa]		Compressive strength [kPa]		Elastic modulus [MPa]
		Cone	Cylinder	Cone	Cylinder	
standard	40	68.6	71.2	54.9	67.6	201
strong	40	183.4	171.0	197.4	169.5	826
cold	41	296.8	290.3	439.1	385.8	1571

3D-printed models

3D-printing offers an easily accessible manufacturing method to produce structures for scaled ice basin tests as it has the potential to rapidly produce several different structural alternatives at a low cost. The cone and cylinder were 3D-printed on a “BigRep ONE”, a large format fused deposition modelling printer. The printing material was polylactic acid. Each structure was made of three parts: a strong, structural part, located at the waterline and designed to withstand ice loads, and two weaker, non-structural extensions, designed to hinder ice from passing above and below the structure. The structural parts had an outer wall thickness of about 2 mm. The infill was varied between 20-40 %. A higher infill percentage was used close to mounting points and at the waterline. Equidistant layers of solid material around the waterline acted as stiffeners to further strengthen it. The non-structural extensions had an outer wall thickness of about 1 mm and an infill of 20 %. After 3D-printing, each part was covered in a polyester body filler. The surfaces were sanded to achieve a smooth texture. Finally, the structures were painted using conventional techniques (Figure 2).

RESULTS

This section presents results on ice failure process and horizontal ice loads, referred to as force or load below, on the structures. The measured force signals were not filtered nor corrected for inertial loading. Based on additional accelerometer measurements it was determined that the inertial loads were negligible.

Ice loads and failure process

Figure 3 shows extracts of the force signal from test runs with the cone and cylinder at 10 mm/s. For the cone, the force signal from “standard” model ice shows clearly defined force peaks, but these peaks flatten and become plateaus in “strong” and “cold” model ice. The force signal for “standard” model ice is characteristic for flexural failure: the force increases linearly up to a peak, followed by a steep drop. The load valleys between peaks indicated ice wedges riding up against before being overturned or falling into the water.

In “strong” and “cold” model ice, the ice failed locally at the ice-structure interface, during the periods indicated by the force plateaus, before undergoing flexural failure. Local failure happened in the form of crushing and spalling. Here, spalling is characterized by abrupt force drops to momentary near-zero load, as the ice sheet is still intact and in contact with the cone. During each spalling event, small ice blocks broke off the ice edge. Several spalling events occurred consecutively before the ice eventually failed in bending. The load peaks associated with spalling failure could be higher than the peak loads associated with flexural failure.

The force signals for the cylinder shows a noisy signal centered around a positive mean force. The variation in the force spectrum is significantly larger in “cold” and “strong” model ice than in “standard” model ice. The force signal from the "strong" model ice exhibits a recurring pattern that is present along with the main force signal. The periodic noise is likely caused by the servo drive of the carriage.

Figures 4 a)-c) show ice wedges created by flexural failure on the cone model. During each test run, the cone lifted the ice sheet over a large radius. In “standard” model ice, the ice rode up only a few centimeters. In “strong” and “cold” model ice, the ice rode up almost the entire slope of the cone. Radial cracks appeared before circumferential cracks led to flexural failure. Only a handful of secondary circumferential cracks were observed.

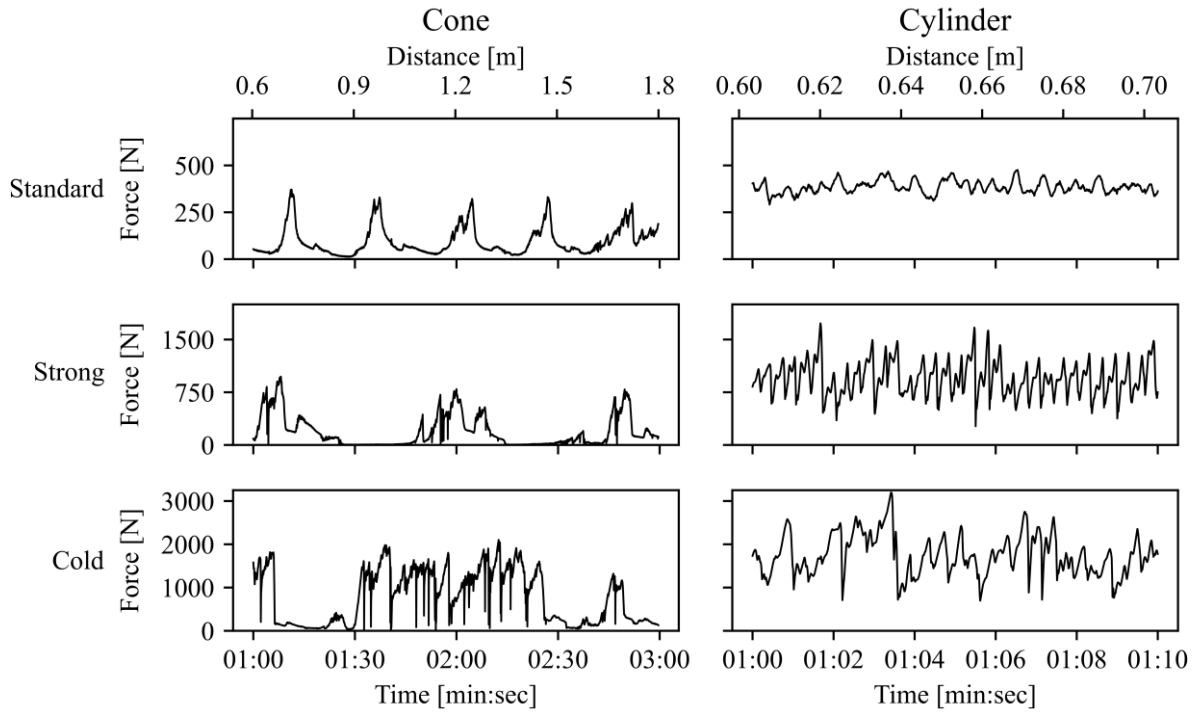

Figure 3. Horizontal force histories from cone and cylinder tests at 10 mm/s.

The length of the radial cracks increased with ice strength: In "standard" model ice, the cracks were less than half a meter long, however their length increased to several meters in "cold" model ice. The long cracks in "strong" and "cold" model ice caused most test runs to be performed in pre-cracked ice sheets. Figure 4 d) shows ice fragments caused by spalling,

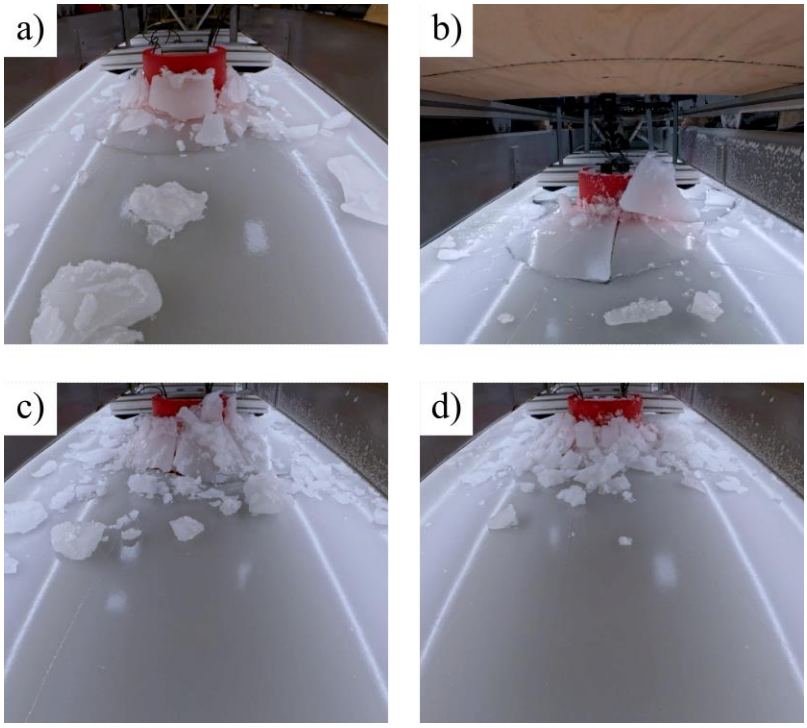

Figure 4. Pictures taken during test runs with the cone model: a) "standard" model ice; b) "strong" model ice; c) "cold" model ice; d) local failure in "cold" model ice.

which are considerably smaller than ice wedges from flexural failure.

Figure 5 presents the mean, standard deviation, and maximum force on the cylinder model at different testing velocities. Overall, the mean was not affected by velocity. The ratio of maximum to mean force was between 1.3-1.6 for “standard”, 1.6-2.4 for “strong”, and 1.7-2.1 for “cold” model ice. The relative standard deviation also increased slightly with increasing velocity, namely 0.08-0.11 for “standard” (except for 20 mm/s), 0.17-0.25 for “strong”, and 0.23-0.29 for “cold” model ice. The ratio of maximum to mean and the relative standard deviation increased gradually with velocity in each ice type, with exception of the relative standard deviation for “standard” model ice at 20 mm/s. The larger relative standard deviation is most likely caused by periodic noise from the servo drive of the carriage.

Figure 6 presents statistics of the peak force, estimated length of ice wedges, and flexural failure frequency on the cone. The length of ice wedges was estimated based on the length of force valleys in the force signal (Figure 3). Force peaks related to flexural failure were selected by hand. Tables 2 and 3 summarize relevant statistics for the peak force and the estimated length of ice wedges. Data points from test runs performed at different velocities were combined as no velocity dependence was observed. The mean estimated length of ice wedges is 0.12 m for “standard” model ice, and it increases to 0.23 m for “strong” model ice and 0.20 m for “cold” model ice. Nonetheless, the results presented in Figure 6 and Tables 2 and 3 are only indicative, especially for “strong” and “cold” ice. Additional experiments with longer run times are needed to improve their accuracy.

Figure 7 summarizes and compares the results from the experiments with the cone and cylinder in different ice sheets. Each plot shows the mean and maximum force on the cylinder and an extract of the force signal on the cone. The ice sheet in which the cylinder was tested varies row-by-row, namely “standard” (top), “strong” (center), and “cold” (bottom). The ice

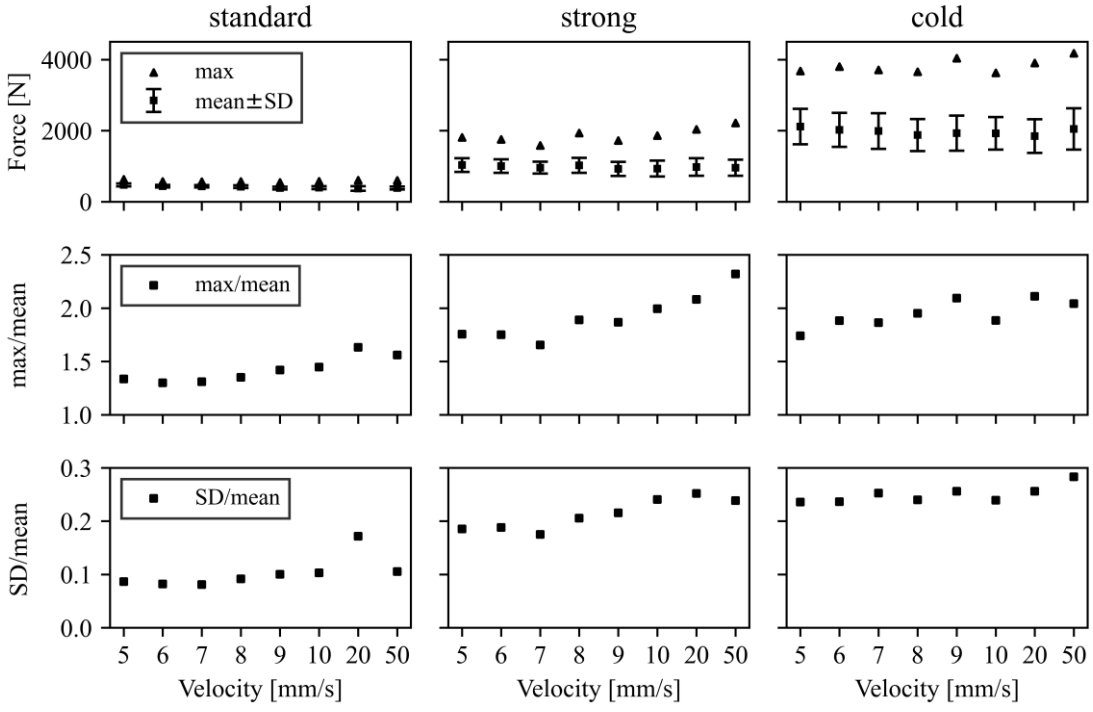

Figure 5. Mean, standard deviation (SD) and maximum force on the cylinder.

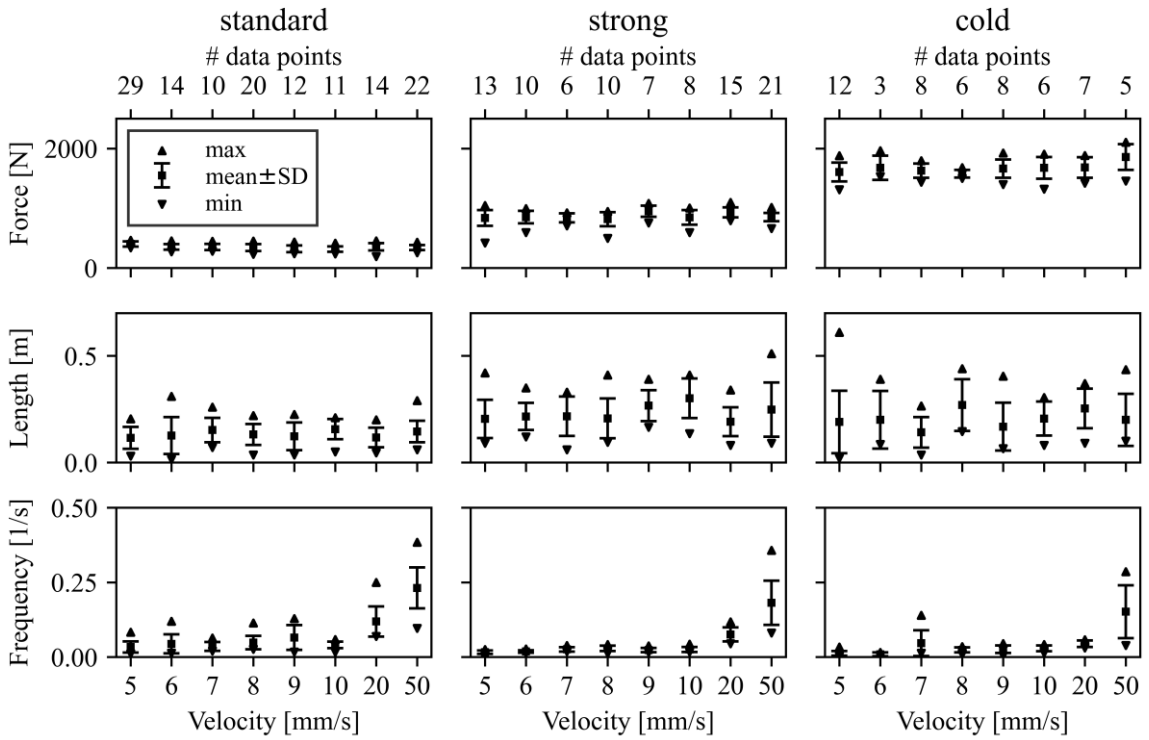

Figure 6. Average, standard deviation, and minimum and maximum values of peaks loads, ice wedge length, and flexural failure frequency on the cone.

sheet in which the cone was tested varies column-by-column, namely “standard” (left), “strong” (middle), and “cold” (right). The plots on the diagonal show results from both structure models tested in the same ice sheet, i.e., “standard” (top), “strong” (middle), and “cold” (bottom). To improve the comparability of test runs with the cylinder and cone model, the strength ratio, R, defined as the ratio of compressive strength (corresponding the cylinder test) to the flexural strength (corresponding to the cone test), is also provided. When R is close to 1, the force peaks on the cone are as close to the mean force on the cylinder. As R increases, the difference between force peaks on the cone and the mean (and maximum) force on the cylinder increases, and vice versa. The plots also show that mixed-mode failure results in lower forces on the cone than crushing failure on the cylinder.

Table 2. Peak force associated with large load drops (excluding spalling events) on the cone.

ice type	mean ± SD [N]	min [N]	max [N]	data points [#]
standard	352±56	191	464	156
strong	864±109	417	1097	96
cold	1661±176	1310	2105	54

Table 3. Statistics of the length of ice wedges (based on experiments with the cone).

ice type	mean ± SD [m]	min [m]	max [m]	data points [#]
standard	0.13±0.06	0.02	0.31	132
strong	0.23±0.10	0.06	0.51	90
cold	0.20±0.12	0.02	0.61	55

Performance of the 3D printed models

The 3D-printed structures performed well in the experiments: no major damage occurred even after the cylinder sustained a peak load of 6 kN in "cold" model ice. The most noticeable issue was that paint was removed when testing in stronger ice sheets. On the cylinder, the paint was removed when testing in "cold" model ice and at 50 mm/s in "strong" model ice. The band of removed paint was located above the waterline, facing the ice. It spanned 180 degrees and had a height of about 25 mm. In the case of the cone model, small patches of paint came off when testing in "cold" model ice. The lower edge of the removed paint coincided with the waterline. The height of the removed paint band was also about 25 mm. The structure surfaces were repaired in-between tests with different ice sheets. When testing the cone in "cold" model ice at 9 mm/s, a large ice wedge became stuck between the ice edge and the non-structural vertical section of the structure. The ice cracked the plastic, leaving three indents. No noticeable peak load was associated with this incident.

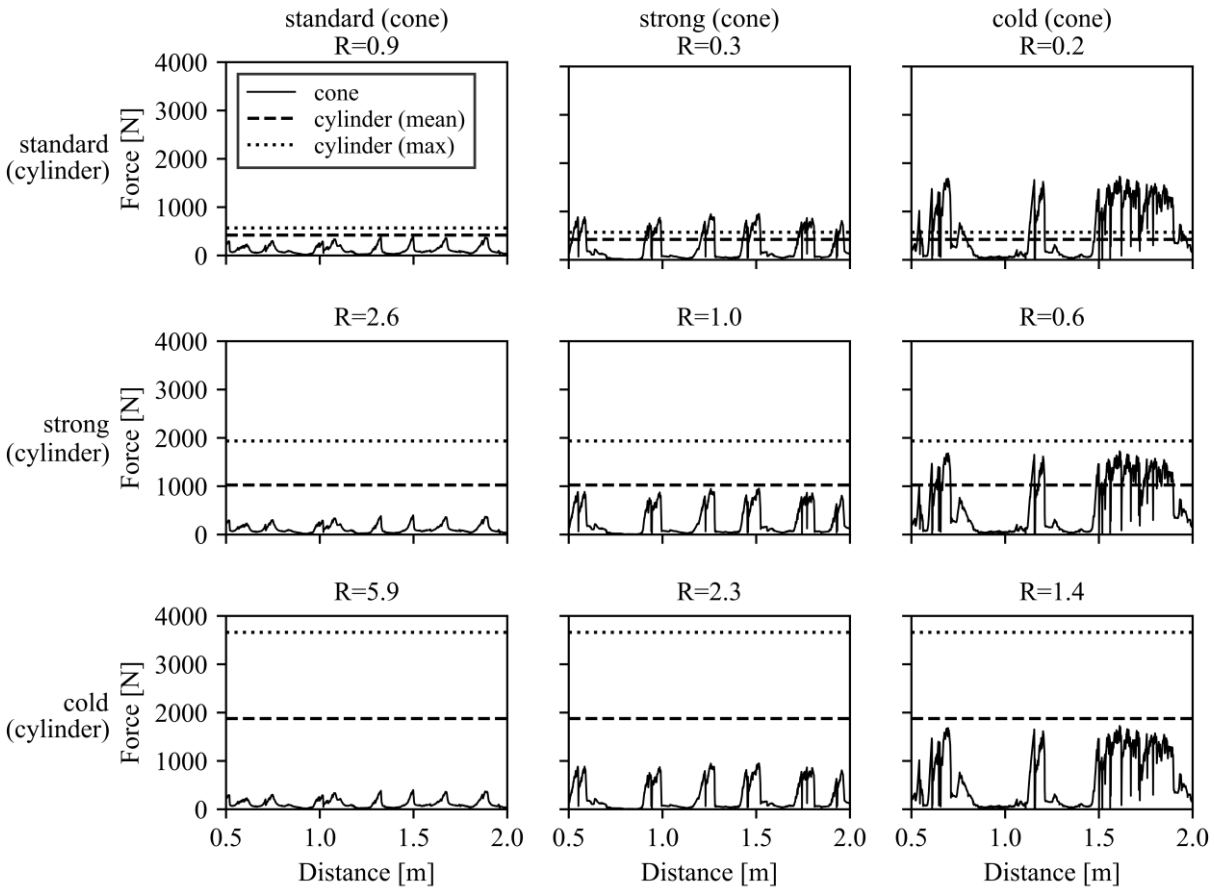

Figure 7. Comparison of the instantaneous force on the cone to the average and maximum force on the cylinder in different model ice types.

DISCUSSION

The experiments successfully achieved mixed-mode ice failure on the cone by increasing the flexural and compressive strength of the model ice. The force measurements showed that the peak force on the cone was equivalent to the average force on the cylinder, while the maximum force on the cylinder was significantly larger. Note that both structures had a different waterline diameter, as they were representative of a monopile foundation and a monopile foundation fitted with an ice cone. Also, the force histories were not corrected for inertia since both test setups had a high enough natural frequency to be considered rigid. Still, the force histories of the cylinder revealed some periodic noise with a frequency around 3 Hz. This noise was likely caused by the servo drive of the carriage to which the test setup was attached.

Force histories on the cone clearly showed that the ice failed in two failure modes (Figures 3 and 7): flexural failure and mixed-mode failure. In “standard” model ice, the ice repeatedly failed in flexural failure, causing ice wedges to break off the ice sheet. In “strong” and “cold” model ice, the ice experienced local failure in the form of crushing and spalling at the ice edge before it eventually failed due to flexural failure. Analyzing and quantifying force peaks and flexural failure frequency was especially difficult in the presence of mixed-mode failure, as both flexural failure and spalling failure showed up as peaks in the recorded signal. Combining results from different test runs performed increased the confidence in the derived statistics. However, longer test runs are needed before conclusions can be drawn. For example, when testing in “cold” model ice, the number of flexural failure events seemed to increase with velocity. With the available information, it is not possible to conclude whether this change in failure frequency was the result of the increased velocity or of the higher density of radial cracks introduced during test runs at lower velocities.

Although mixed-mode failure was observed when testing the cone in “strong” and “cold” model ice, the question remains whether the model-scale ice conditions can be compared to full-scale conditions. The strength ratio of “standard”, “strong”, and “cold” model ice was 0.9, 1.0, and 1.4, respectively. Sea ice is commonly thought to have a strength ratio around 3. Suominen et al. (2019) found a mean strength ratio of 2.7 (with a standard deviation of 0.5) based on selected compressive strength data in Kellner et al. (2019) and flexural strength values derived using a regression formula (Timco & O’Brien, 1994). Measurements performed by von Bock und Polach (2010) in the Bay of Bothnia (64°20.778’N, 22°13.805’E) resulted in a ratio of 1.6. Compared to these results, the strength ratios of the different types of model ice are low, with “cold” model ice having the largest, and therefore most representative, strength ratio. Since mixed-mode failure was observed in “cold” model ice, it may also happen in full-scale against similar cones.

Moreover, Figure 7 shows that the difference between the mean and maximum force on the cylinder and the peak force on the cone increases as the strength ratio increases. If the cone and cylinder had been tested in an ice sheet with a higher strength ratio, it is possible that the ice would have undergone flexural failure before conditions for local crushing failure were met. Nonetheless, the strength ratio alone is not sufficient to define conditions in which mixed-mode failure can occur. No mixed-mode failure was observed in “standard” model ice, even though the strength ratio was below 1. Figure 4 showed that “standard” model ice had a lower maximum to mean force ratio and relative standard deviation than the other ice types. The difference in the variation of the force measurements indicates that its failure mechanism is different from that of the "cold" model ice, which has been shown to in brittle crushing in

experiments by Hendrikse et al. (2022). Therefore, "standard" model ice may not be suitable in model-scale tests aimed at analyzing crushing or mixed-mode failure.

To summarize, model-scale experiments focused on mixed-mode failure require model ice with a representative strength ratio, scaled flexural and compressive strength and the ability to fail in brittle crushing. Depending on the model ice, it may not be possible to fulfill all criteria with the same ice sheet. Nonetheless, test results from different ice sheets, each focused on one aspect of the ice failure process, may be combined to gain a better understanding of the different ice failure modes on the structure and the conditions when they occur. For instance, the current experiments show that mixed-mode failure can occur on an upward bending cone with a 60-degree cone angle, however the necessary ice conditions are only met if the ice has a low strength ratio. With higher strength ratios, the ice will likely only undergo flexural failure.

Lastly, 3D-printed cylinder and cone models withstood the ice load and the cold environment in the ice basin. Nonetheless, the current design presented two limitations: some of the paint and filler material was removed when testing in “strong” and “cold” model ice, and an ice wedge cracked the cone locally. These issues were small and easily repairable, and they will be addressed in the next design iteration. Nonetheless, these issues provided insight into the ice-structure interaction process. On both structures, the width of the removed paint strip was 25 mm high, which is narrower than the ice sheet itself. On the cone, the band of removed paint followed the waterline, suggesting that ice crushed before it started to ride-up the inclined slope.

CONCLUSION

Preliminary ice basin experiments were performed to investigate the effect of varying mechanical properties of model ice on the ice failure process against two 3D-printed structures representative of offshore wind turbine foundations: a cylinder and a cone. Each structure was tested at eight different velocities, ranging from 5 mm/s to 50 mm/s, in three different ice sheets. In “standard” model ice, the ice failed in crushing against the cylinder and in bending against the cone. In “strong” and “cold” model ice, the ice failed in brittle crushing against the cylinder and in mixed-mode failure, consisting of crushing, spalling, and bending, against the cone. To perform scalable experiments focused on mixed-mode failure against cones, the model ice should have scaled flexural and compressive strength, a representative compressive to flexural strength ratio, and the ability to fail in brittle crushing. If these conditions cannot be met, it may be possible to combine experimental results from tests performed in multiple ice sheets, each focused on one aspect of the ice failure process. Additionally, the experiments show that 3D printed structures are suitable for model-scale experiments in an ice basin.

ACKNOWLEDGEMENTS

AP, AP, and OP would like to acknowledge the financial support from the Academy of Finland research project (348586) “WindySea - Modelling engine to design, assess environmental impacts, and operate wind farms for ice-covered waters”. All authors would like to thank Teemu Päivärinta and Lasse Turja from the Aalto Ice and Wave Tank for their help preparing and installing the test setup and executing the experiments. From the Aalto University School of Arts, Design and Architecture we would like to thank Hector Velasquez Reynoso, and Darren Bratten of the 3D printing workshop for their help in designing and 3D-printing the model structures, and Kari Kääriäinen from the Waterjet cutting workshop.

REFERENCES

Cornett, A.M., & Timco, G.W., 1998. Ice loads on an elastic model of the Molikpaq. *Applied Ocean Research*, 20(1-2), pp.105-118.

Croasdale, K., & Allyn, N., 2018. Ridge Loads on Wind Turbine Structures, *OTC Arctic Technology Conference*.

Hammer, T.C., Willems, T., & Hendrikse, H., 2023. Dynamic ice loads for offshore wind support structure design. *Marine Structures*, 87, p.103335.

Hendrikse, H., Hammer, T.C., Owen, C.C., van den Berg, M., van Beek, K., Polojärvi, A., Puolakka, O., & Willems, T., 2022a. Ice basin tests for ice-induced vibrations of offshore structures in the SHIVER project, *Proceedings of the ASME 2022 41st International Conference on Ocean, Offshore and Arctic Engineering*.

Hendrikse, H., Hammer, T.C., van den Berg, M., Willems, T., Owen, C.C., van Beek, K., Ebben, N.J.J., Puolakka, O., & Polojärvi, A., 2022b. Experimental data from ice basin tests with vertically sided cylindrical structures. *Data in Brief,* 41, p. 107877.

Jiang, Z., Heinonen, J., Tikanmäki, M., Mikkola, E., Perälä, I., Shestov, A., Høyland, K.V., Salganik, E., van den Berg, M., Li, H., & Ervik, Å., 2021. Scale-model ridges and interaction with narrow structures, Part 4 Global loads and failure mechanisms, *Proceedings of the 26th International Conference on Port and Ocean Engineering under Arctic Conditions.*

Kellner, L., Stender, M., Herrnring, H., Ehlers, S., Hoffmann, N., & Høyland, K.V., 2019. Establishing a common database of ice experiments and using machine learning to understand and predict ice behavior. *Cold Regions Science and Technology*, 162, pp.56-73.

Li, Z., & Riska, K., 1996. *Preliminary Study of Physical and Mechanical Properties of Model Ice,* Espoo, Finland: Helsinki University of Technology.

Nord, T.S., Samardžija, I., Hendrikse, H., Bjerkås, M., Høyland, K.V., & Li, H., 2018. Ice-induced vibrations of the Norströmsgrund lighthouse. *Cold Regions Science and Technology*, 155, pp.237-251.

Saeki, H., Hiyayama, K.I., Kawasaki, T., Akagawa, S., Kato, K., Kamesaki, K., Saka, K., & Kurokawa, A., 1996. JOIA project of study on ice load, *Proceedings of the 13th IAHR International Symposium on Ice*, 1, pp. 17-27.

Suominen, M.T., von Bock und Polach, R.U.F., & Haase, A., 2019. The effect of sample dimensions on the compressive strength of model-scale ice, *Proceedings of the 25th International Conference on Port and Ocean Engineering under Arctic Conditions.*

Tian, Y., Huang, Y. & Li, W., 2019. Experimental Investigations on Ice Induced Vibrations of a Monopile-type Offshore Wind Turbine in Bohai Sea. *Proceedings of the 29th International Offshore and Polar Engineering Conference*.

Timco, G.W., & O.'Brien, S., 1994. Flexural strength equation for sea ice. *Cold Regions Science and Technology*, 22(3), pp.285-298.

von Bock und Polach, R.U.F., 2010. *Investigation on employing ships as sensors for ice thickness measurements*, Finland, Espoo: Aalto University, School of Science and Technology, Faculty of Engineering and Architecture, Department of Applied Mechanics.

WindEurope, 2022. *Baltic Sea Countries sign declaration for more cooperation in offshore wind.* [Online] Available at: https://windeurope.org/newsroom/press-releases/baltic-sea-countries-sign-declaration-for-more-cooperation-in-offshore-wind/ [Accessed 8 March 2023].

Yue, Q., Guo, F., & Kärnä, T., 2009. Dynamic ice forces of slender vertical structures due to ice crushing. *Cold Regions Science and Technology*, 56(2-3), pp.77-83.

Ziemer, G., Evers, K.-U., & Voosen, C., 2015. Influence of structural compliance and slope angle on ice loads and dynamic response of conical structures, *Proceedings of the ASME 2015 34th International Conference on Ocean, Offshore and Arctic Engineering*.

Ziemer, G., Stange, T., & Hisette, Q., 2022. HSVA Model Ice - A Status Report, *Proceedings of the ASME 2022 41st International Conference on Ocean, Offshore and Arctic Engineering*.